

Predictive Control of an Autonomous Ground Vehicle using an Iterative Linearization Approach

Ashwin Carvalho*, Yiqi Gao*, Andrew Gray*, H. Eric Tseng†, Francesco Borrelli*

* Department of Mechanical Engineering, University of California at Berkeley, CA, U.S.A.

† Powertrain Control R&A, Ford Motor Company, Dearborn, MI, U.S.A.

Abstract—This paper presents the design of a controller for an autonomous ground vehicle. The goal is to track the lane centerline while avoiding collisions with obstacles. A nonlinear model predictive control (MPC) framework is used where the control inputs are the front steering angle and the braking torques at the four wheels. The focus of this work is on the development of a tailored algorithm for solving the nonlinear MPC problem. Hardware-in-the-loop simulations with the proposed algorithm show a reduction in the computational time as compared to general purpose nonlinear solvers. Experimental tests on a passenger vehicle at high speeds on low friction road surfaces show the effectiveness of the proposed algorithm.

I. INTRODUCTION

Recent advances in control and sensing technologies have led to the development of several active safety systems in automobiles. Driver assistance systems such as adaptive cruise control and lane-keeping assistance attempt to keep the vehicle safe by correcting the driver's steering and braking inputs [1]–[3]. At the extreme end of the intelligent vehicle spectrum are autonomous vehicles in which the controller has complete control of the vehicle [4]–[6]. The underlying challenges in the control of fully autonomous and semi-autonomous vehicles are fundamentally similar. The focus of this work is on the former.

Two main elements make the autonomous vehicle control problem nontrivial: (1) the nonlinearity of the vehicle dynamics, and (2) the presence of time-varying state and input constraints while navigating in a dynamic environment. Because of its ability to handle system nonlinearities and constraints in a unified manner, model predictive control (MPC) has been shown to be an attractive control methodology in this class of applications [2]–[5], [7]–[9].

The main limitation in using optimization-based control strategies, such as MPC, is the computational burden of solving the optimization problem in real-time. The complexity arises from the nonlinearity of the vehicle dynamics and the non-convexity of the constraints [8]. While linearizing the system dynamics leads to some of the constraints becoming convex, the collision avoidance constraints are still non-convex. Moreover, a linearized vehicle model is a good approximation only in a small region around the reference state and input vectors about which the linearization is performed. The use of nonlinear MPC for vehicle control has been proposed in [2]–[4], [7], [8]. General purpose solvers for nonlinear optimization, such as NPSOL [10], are used to solve the resulting non-convex optimization problem.

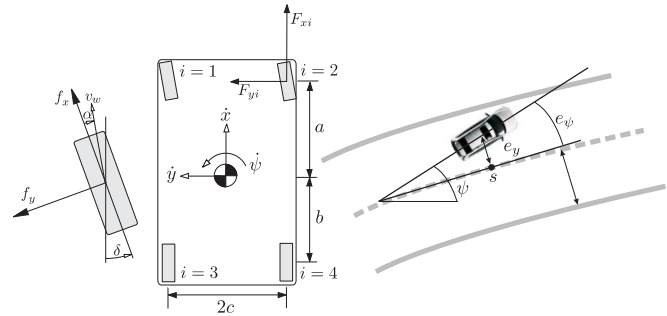


Fig. 1: Notation used in vehicle model

In this work, we propose a customized sequential quadratic programming (SQP) algorithm which exploits the structure of the problem of interest. SQP involves the iterative solution of a convex approximation to the original problem [11]–[13]. In the proposed approach, the nonlinear vehicle dynamics are linearized analytically, and a convex approximation to the collision avoidance constraints is obtained. Simulation and experimental results show the effectiveness of such a tailored approach in reducing the online computational time as compared to a generic nonlinear solver.

The paper is organized as follows. Section II describes the vehicle model, Section III describes the system constraints, Section IV presents the formulation of the MPC problem, Section V details the proposed algorithm, Section VI shows results from hardware-in-the-loop (HIL) simulations, experimental results are presented in Section VII, and concluding remarks are made in Section VIII.

II. VEHICLE DYNAMICS MODEL

A four wheel nonlinear vehicle model is used for the control design. The notation used in the vehicle model is depicted in Figure 1. The following set of nonlinear differential equations are used to describe the motion of the vehicle,

$$\ddot{x} = \dot{y}\dot{\psi} + \frac{1}{m} \sum_{i=1}^4 F_{x_i} \quad (1a)$$

$$\ddot{y} = -\dot{x}\dot{\psi} + \frac{1}{m} \sum_{i=1}^4 F_{y_i} \quad (1b)$$

$$\ddot{\psi} = \frac{1}{I_z} (a(F_{y_1} + F_{y_2}) - b(F_{y_3} + F_{y_4}))$$

$$+ c(-F_{x_1} + F_{x_2} - F_{x_3} + F_{x_4})) \quad (1c)$$

$$\dot{e}_\psi = \dot{\psi} - \kappa \dot{s} \quad (1d)$$

$$\dot{e}_y = \dot{x} \sin(e_\psi) + \dot{y} \cos(e_\psi) \quad (1e)$$

$$\dot{s} = \frac{1}{1 - \kappa e_y} (\dot{x} \cos(e_\psi) - \dot{y} \sin(e_\psi)), \quad (1f)$$

where m and I_z denote the vehicle mass and yaw inertia, respectively, a and b denote the distances from the vehicle's center of gravity to the front and rear axles, respectively, and c denotes the vehicle's half track-width. \dot{x} and \dot{y} denote the longitudinal and lateral speeds in the body frame, respectively, and $\dot{\psi}$ denotes the yaw rate. e_y and e_ψ denote the lateral position error and angular error with respect to the road centerline, respectively, κ denotes the curvature of the road, and s denotes the longitudinal position of the vehicle along the road. The longitudinal and lateral forces in the body frame F_{x_i} and F_{y_i} , respectively, are given by,

$$F_{x_i} = f_{x_i} \cos(\delta_i) - f_{y_i} \sin(\delta_i) \quad (2a)$$

$$F_{y_i} = f_{x_i} \sin(\delta_i) + f_{y_i} \cos(\delta_i), \quad (2b)$$

where f_{x_i} and f_{y_i} are the longitudinal and lateral forces in the coordinate frame aligned with the tire axes, and δ_i is the steering angle at wheel i . The following assumption is introduced on the steering angles,

Assumption 1. Only the front wheels can be steered, and the steering angles at the front left and right wheels are equal, i.e., $\delta_1 = \delta_2 = \delta_f$, and $\delta_3 = \delta_4 = 0$.

The longitudinal forces f_{x_i} are given by,

$$f_{x_i} = \beta_i \mu_i F_{z_i}, \quad (3)$$

where β_i is referred to as the braking ratio, μ_i denotes the friction coefficient between the tire and the road surface, and F_{z_i} denotes the normal force between the tire and the road. $\beta_i = -1$ corresponds to full braking, and $\beta_i = 1$ corresponds to full throttle. The following assumption is introduced on the braking ratios,

Assumption 2. The braking ratio at the front left (right) wheel is equal to that at the rear left (right) wheel, i.e., $\beta_1 = \beta_3 = \beta_l$, and $\beta_2 = \beta_4 = \beta_r$.

The lateral forces f_{y_i} are modeled using a modified nonlinear Fiala tire model [14] as,

$$f_{y_i} = \begin{cases} -C_{\alpha_i} \tan(\alpha_i) + \frac{C_{\alpha_i}^2}{3\eta_i \mu_i F_{z_i}} |\tan(\alpha_i)| \tan(\alpha_i) \\ -\frac{C_{\alpha_i}^3}{27\eta_i^2 \mu_i^2 F_{z_i}^2} \tan^3(\alpha_i), & \text{if } |\alpha_i| < \alpha_{sl_i} \\ -\eta_i \mu_i F_{z_i} \text{sign}(\alpha_i), & \text{if } |\alpha_i| \geq \alpha_{sl_i}, \end{cases} \quad (4)$$

where α_i denotes the tire slip angle, C_{α_i} denotes the tire cornering stiffness, $\eta_i = \sqrt{1 - \beta_i^2}$, and $\alpha_{sl_i} = \tan^{-1}(\frac{3\eta_i \mu_i F_{z_i}}{C_{\alpha_i}})$ is the tire slip angle at which maximum lateral force is obtained. The slip angles α_i are given by,

$$\alpha_i = \tan^{-1}\left(\frac{v_{c_i}}{v_{l_i}}\right), \quad (5)$$

where,

$$v_{c_i} = v_{y_i} \cos(\delta_i) - v_{x_i} \sin(\delta_i) \quad (6a)$$

$$v_{l_i} = v_{y_i} \sin(\delta_i) + v_{x_i} \cos(\delta_i) \quad (6b)$$

$$\begin{aligned} v_{y_{1,2}} &= \dot{y} + a\dot{\psi} & v_{y_{3,4}} &= \dot{y} - b\dot{\psi} \\ v_{x_{1,2}} &= \dot{x} - c\dot{\psi} & v_{x_{3,4}} &= \dot{x} + c\dot{\psi}. \end{aligned} \quad (6c)$$

The following assumptions are introduced,

Assumption 3. The normal forces F_{z_i} are constant, and determined by the static weight distribution of the vehicle.

Assumption 4. The friction coefficient μ_i is known at each time step, and is constant over a finite time horizon.

Assumption 5. The road curvature κ is known as a function of the longitudinal position s of the vehicle along the road.

The nonlinear vehicle dynamics given by (1)–(4) can be compactly written as,

$$\dot{z}(t) = f(z(t), u(t), w(t)), \quad (7)$$

where $z = [\dot{x}, \dot{y}, \dot{\psi}, e_\psi, e_y, s]^T$, $u = [\delta_f, \beta_l, \beta_r]^T$, and $w = [\mu, \kappa]^T$ are the state, input and parameter vectors, respectively.

III. SAFETY CONSTRAINTS

The goal of keeping the vehicle in the lane while avoiding obstacles and operating in a stable region can be expressed as constraints on the vehicle's states and inputs.

The requirement that the vehicle stays within the lane can be expressed as,

$$e_{y,\min}^{\text{lane}} \leq e_y \leq e_{y,\max}^{\text{lane}}, \quad (8)$$

where the bounds $e_{y,\min}^{\text{lane}}$ and $e_{y,\max}^{\text{lane}}$ account for the width of the vehicle.

Physical limitations on the actuators impose bounds on the control inputs and input rates,

$$\delta_{f,\min} \leq \delta_f \leq \delta_{f,\max} \quad (9a)$$

$$\dot{\delta}_{f,\min} \leq \dot{\delta}_f \leq \dot{\delta}_{f,\max} \quad (9b)$$

$$-1 \leq \beta_{\min} \leq \beta_l, \beta_r \leq \beta_{\max} \leq 1. \quad (9c)$$

We would like the vehicle to operate in a stable region in which it is easily maneuverable by a normally skilled driver. This can be enforced by requiring the tire slip angles to be small. We only impose constraints on the front wheel slip angles, since we can “directly” control them by means of the front steering angle. The resulting constraints can be expressed as,

$$-\alpha_{sl_i} \leq \alpha_{i,\min} \leq \alpha_i \leq \alpha_{i,\max} \leq \alpha_{sl_i}. \quad (i = 1, 2) \quad (10)$$

Finally, the vehicle must avoid collisions with obstacles in the environment. We introduce the following assumption,

Assumption 6. The current and future positions of all obstacles in the vicinity of the vehicle are known as a function of time.

The method presented in [8], [9] is used to formulate collision avoidance constraints. Obstacles in the environment are mapped into a region of the road in which the vehicle can move safely. The boundaries of this region are assumed

to be known a-priori as a function of time and the distance along the road. Let $e_y^L(d, t)$ and $e_y^U(d, t)$ denote the distance of the lower and upper boundaries, respectively, from the road centerline, where d is the longitudinal position along the road. The collision avoidance constraints can then be expressed as,

$$e_y^L(s(t), t) \leq e_y(t) \leq e_y^U(s(t), t). \quad (11)$$

Note that the constraints given by (11) are non-convex and non-differentiable in general due to the nonlinear dependence of the bounds e_y^L and e_y^U on s . The safety constraints (8)–(11) can be compactly written as,

$$h(z(t), u(t), w(t)) \leq 0. \quad (12)$$

IV. MODEL PREDICTIVE CONTROL (MPC) FORMULATION

The problem of generating feasible trajectories for an autonomous vehicle can be formulated as an MPC problem. At each sampling time instant, a constrained finite-time optimal control problem is solved to determine a sequence of control inputs which minimizes a given cost function. Only the first input of the optimal input sequence is applied to the system. This process is repeated at the next sampling time instant using the new measurements. The optimization problem to be solved at each time step is given by,

$$\min_{\mathcal{U}_t} \sum_{k=0}^{H_p} \|Q(z_{t+k,t} - z_{ref,k})\|_2^2 + \sum_{k=0}^{H_p-1} \|Ru_{t+k,t}\|_2^2 \quad (13a)$$

$$\text{s.t. } z_{t+k+1,t} = f_d(z_{t+k,t}, u_{t+k,t}, w_{t+k,t}) \quad (13b)$$

$$h(z_{t+k,t}, u_{t+k,t}, w_{t+k,t}) \leq 0 \quad (13c)$$

$$(k = 0, \dots, H_p - 1)$$

$$z_{t,t} = z(t), \quad (13d)$$

where t denotes the current time instant, H_p denotes the prediction horizon, and $z_{t+k,t}$ denotes the predicted state at time $t+k$ obtained by applying the control input sequence $\mathcal{U}_t = \{u_{t+k,t}\}_{k=0}^{H_p-1}$ to the system with the initial condition $z_{t,t} = z(t)$. The constraint (13b) is obtained by discretizing the equations of motion (7). The reference state sequence $\{z_{ref,k}\}_{k=0}^{H_p}$ encodes control objectives such as tracking the lane centerline and maintaining a desired speed.

The computational complexity of the MPC problem can be reduced by keeping the input vectors constant for every H_i steps in the prediction horizon. That is,

$$u_{t+i \cdot H_i+k,t} = u_{t+i \cdot H_i,t} \quad \forall k = 0, \dots, (H_i - 1), \quad (14)$$

$$\forall i = 0, \dots, (H_p/H_i).$$

This reduces the number of optimization variables in (13) by a factor of H_i . We refer to the parameters H_p and H_i as the prediction horizon and the input blocking factor, respectively.

V. ITERATIVE LINEARIZATION APPROACH

We now present a tailored algorithm for solving (13). In the following sections, we use x_k to denote the variable $x_{t+k,t}$, where x can be z , u or w .

A. Overview

The proposed algorithm is similar in structure to an SQP approach [11]–[13]. The main difference lies in the convexification scheme at each iteration. Recall that the optimization problem (13) is non-convex due to the nonlinearity of the dynamics map $f_d(\cdot)$ in (13b), and the non-convexity of the collision avoidance constraints (11). Hence, we analytically linearize the vehicle dynamics model, and simplify the collision avoidance constraints to obtain a QP approximation to the original problem. Such an approach is expected to be faster than a numerical convexification scheme.

We introduce the following notation. Let $\bar{\mathcal{U}}_t$ denote the current candidate solution to the optimization problem (13). Let $\bar{\mathcal{Z}}_t = \{\bar{z}_k\}_{k=0}^{H_p}$ and $\{\bar{w}_k\}_{k=0}^{H_p-1}$ be the sequences of predicted states and parameters, respectively, generated by the nonlinear vehicle model (13b) with the input sequence $\bar{\mathcal{U}}_t$ and $\bar{z}_0 = z(t)$ as the initial condition. A method of approximately convexifying constraints, given $\bar{\mathcal{U}}_t$ and $\bar{\mathcal{Z}}_t$, is presented in the next section.

B. Convexification of constraints

1) *Vehicle dynamics*: The nonlinear model (7) can be linearized about $\bar{\mathcal{U}}_t$ and $\bar{\mathcal{Z}}_t$ to yield a linear time-varying (LTV) state-space representation,

$$\delta z_{k+1} = A(\bar{z}_k, \bar{u}_k, \bar{w}_k) \delta z_k + B(\bar{z}_k, \bar{u}_k, \bar{w}_k) \delta u_k \quad (15)$$

$$\delta z_0 = 0, \quad (k = 0, \dots, H_p - 1)$$

where δz_k and δu_k denote the deviation of the states and inputs from \bar{z}_k and \bar{u}_k , respectively, and,

$$A(\bar{z}_k, \bar{u}_k, \bar{w}_k) = \nabla_z f_d(\bar{z}_k, \bar{u}_k, \bar{w}_k) \quad (16a)$$

$$B(\bar{z}_k, \bar{u}_k, \bar{w}_k) = \nabla_u f_d(\bar{z}_k, \bar{u}_k, \bar{w}_k). \quad (16b)$$

Analytical expressions for the maps $A(\cdot)$ and $B(\cdot)$ are determined offline using (1)–(4).

2) *Safety constraints*: Recall that the collision avoidance constraints as formulated in (11) are non-differentiable in general. We write the approximate collision avoidance constraints as,

$$e_y^L(\bar{s}_k, t+k) \leq e_{y_k} \leq e_y^U(\bar{s}_k, t+k), \quad (17)$$

$$(k = 0, \dots, H_p - 1)$$

where \bar{s}_k is a component of the state vector \bar{z}_k . Note that the only difference between (11) and (17) is the use of \bar{s} in (17) instead of s in (11) to sample the boundaries of the safe region. This results in simple bounds on e_y . The approximate constraints (17) converge to the actual constraints (11) as δz_k converges to 0.

Let $\bar{h}(\cdot)$ be the map obtained by replacing the collision avoidance constraints (11) in $h(\cdot)$ with (17). The linearized safety constraints can then be expressed as,

$$C(\bar{z}_k, \bar{u}_k, \bar{w}_k) \delta z_k + D(\bar{z}_k, \bar{u}_k, \bar{w}_k) \delta u_k + E(\bar{z}_k, \bar{u}_k, \bar{w}_k) \leq 0, \quad (18)$$

$$(k = 0, \dots, H_p - 1)$$

where,

$$C(\bar{z}_k, \bar{u}_k, \bar{w}_k) = \nabla_z \bar{h}(\bar{z}_k, \bar{u}_k, \bar{w}_k) \quad (19a)$$

$$D(\bar{z}_k, \bar{u}_k, \bar{w}_k) = \nabla_u \bar{h}(\bar{z}_k, \bar{u}_k, \bar{w}_k) \quad (19b)$$

$$E(\bar{z}_k, \bar{u}_k, \bar{w}_k) = \bar{h}(\bar{z}_k, \bar{u}_k, \bar{w}_k). \quad (19c)$$

Analytical expressions for the maps $C(\cdot)$, $D(\cdot)$ and $E(\cdot)$ are determined offline.

C. QP formulation

The convexification methodology presented in V-B transforms the non-convex optimization problem (13) into a QP subproblem given by,

$$\min_{\delta \mathcal{U}_t, \epsilon} \sum_{k=0}^{H_p} \|Q(\bar{z}_k + \delta z_k - z_{ref,k})\|_2^2 \quad (20a)$$

$$+ \sum_{k=0}^{H_p-1} (\|R(\bar{u}_k + \delta u_k)\|_2^2 + \|\bar{R}\delta u_k\|_2^2) + c^T \epsilon$$

$$\text{s.t. } \delta z_{k+1} = A(\bar{z}_k, \bar{u}_k, \bar{w}_k)\delta z_k + B(\bar{z}_t, \bar{u}_t, \bar{w}_k)\delta u_k \quad (20b)$$

$$C(\bar{z}_k, \bar{u}_k, \bar{w}_k)\delta z_k + D(\bar{z}_k, \bar{u}_k, \bar{w}_k)\delta u_k + E(\bar{z}_k, \bar{u}_k, \bar{w}_k) \leq M\epsilon \quad (20c)$$

$$\|\delta u_k\| \leq \epsilon_{u,tr} \quad (20d)$$

$$(k = 0, \dots, H_p - 1)$$

$$\delta z_0 = 0. \quad (20e)$$

The additional term in the objective function (20a) penalizes the deviation δu_k from \bar{u}_k in order to improve the convergence of the algorithm. A trust region-like constraint (20d) is also introduced to ensure the accuracy of the linear model (20c) around \bar{U}_t and \bar{Z}_t . The linearized safety constraints (19a) are imposed as soft constraints by introducing the slack variable ϵ in (20c). The slack variable is penalized linearly in (20a), where $c \gg Q, R, \bar{R}$.

D. Overall algorithm

The nonlinear constrained finite-time optimal control problem (13) is solved in a receding horizon manner by using Algorithm 1. N_{max} limits the maximum number of iterations of the iterative linearization procedure. The function $warmStart(\cdot)$ uses the optimal input sequence \bar{U}_{t-1} from the previous time step to generate an initial candidate input sequence \bar{U}_t for the current time step as follows,

$$\bar{u}_{t+k,t} = \begin{cases} \bar{u}_{t+k,t-1}, & \text{if } k = 0, 1, \dots, (H_p - 2) \\ \bar{u}_{t+H_p-2,t-1}, & \text{if } k = H_p - 1. \end{cases} \quad (21)$$

The function $simSys(\cdot)$ generates the state sequence \bar{Z}_t using the nonlinear vehicle model (13b). The function $solveQP(\cdot)$ formulates the QP (20) using \bar{U}_t and \bar{Z}_t (as presented in Section V-B), and yields the perturbed input sequence $\delta \mathcal{U}_t = \{\delta u_k\}_{k=0}^{H_p-1}$. The algorithm terminates when the norm of the perturbations is small.

Algorithm 1 Tailored MPC algorithm

```

 $\bar{U}_0 = 0$ 
while  $t \geq 0$  do
     $z_{t,t} = z(t)$  ▷ Measure state
     $\bar{U}_t = warmStart(\bar{U}_{t-1})$  ▷ Initialize candidate
     $i = 0$  ▷ Iteration number
    while  $\|\delta \mathcal{U}_t\| > \epsilon_u$  and  $i < N_{max}$  do
         $\bar{Z}_t = simSys(z_{t,t}, \bar{U}_t)$  ▷ Simulate system
         $\delta \mathcal{U}_t = solveQP(\bar{U}_t, \bar{Z}_t)$  ▷ Solve QP (20)
         $\bar{U}_t = \bar{U}_t + \delta \mathcal{U}_t$  ▷ Update candidate
         $i = i + 1$ 
    end while
     $u^*(t) = \bar{u}_{t,t}$  ▷ Apply input
     $t = t + 1$ 
end while

```

VI. SIMULATION RESULTS

We now compare the performance of the proposed controller with that of the controller which uses the general purpose nonlinear solver NPSOL. Note that NPSOL implements a sequential quadratic programming (SQP) algorithm for nonlinear optimization [10], and that the internal QP solver used by NPSOL (i.e. LSSOL) is the same as that used by the proposed algorithm.

A. Simulation setup description

HIL simulations of the controller are performed on a dSPACE rapid prototyping system consisting of a DS1401 MicroAutoBox (IBM PowerPC 750FX processor, 800 MHz) and a DS1006 processor board (Quad-core AMD Opteron processor, 2.8 GHz). The controller runs on the MicroAutoBox, and the DS1006 board simulates the vehicle dynamics using a nonlinear four wheel vehicle model with a Pacejka tire model. The vehicle parameters are as follows: $m = 2050$ kg, $I_z = 3344$ kg-m², $a = 1.432$ m, $b = 1.472$ m, $c = 0.8125$ m. The control actions are executed at 10 Hz.

B. Results and discussion

We denote the controller which uses the proposed iterative linearization scheme as Controller 1, and the controller which uses NPSOL as Controller 2. Note that both controllers are solving the nonlinear problem (13) with identical safety constraints. That is, the complexity of the optimization problem solved by both controllers is the same in terms of the number of optimization variables and constraints. The simulation results are summarized in Figures 2–3.

The scenario consists of a single obstacle in the path of the vehicle. The road is straight and the edge of the obstacle is at a distance of 2 m from the road centerline. In order to account for the width of the vehicle, a tolerance of 1 m is included in the obstacle and lane bounds. A triangular zone is appended to the front of the obstacle to avoid aggressive maneuvers. We assume the existence of a high-level decision making module which decides the side of the obstacle on which the vehicle must pass. The entry speed of the vehicle is 15 m/s.

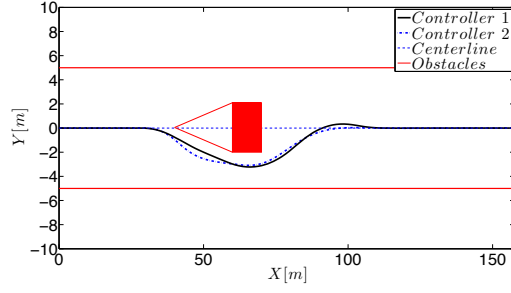


Fig. 2: Simulation 1: The performance of the proposed controller (controller 1) is similar to that of the controller which uses NPSOL (controller 2) for the same sampling time, prediction horizon, environment scenario and constraints in the optimization problem.

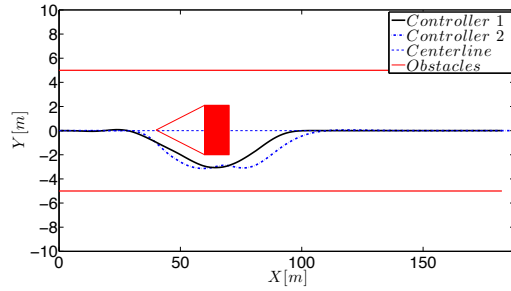


Fig. 3: Simulation 2: Controller 1 uses a much longer prediction horizon as compared to controller 2.

In Simulation 1, the performance of the two controllers is compared when the same prediction horizon and input blocking factor are used ($H_p = 9$, $H_i = 3$). The path of the vehicle is shown in Figure 2. The performance of the two controllers is observed to be similar.

In Simulation 2, the prediction horizon for controller 1 is increased to $H_p = 30$, while that for controller 2 is increased to $H_p = 11$. The path of the vehicle is shown in Figure 3.

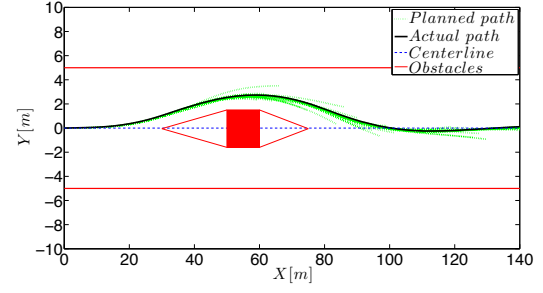
Remark 1. The prediction horizon used in Simulation 2 is the maximum allowable given the 100 ms sampling time.

It is seen that the vehicle stays very close to the obstacle while using controller 1, and returns to the road centerline with almost no overshoot. However, controller 2 does not improve its performance compared to Simulation 1. Moreover, the proposed methodology allows the use of a much longer prediction horizon as compared to the approach that uses NPSOL. This is desirable for the early consideration of hazards.

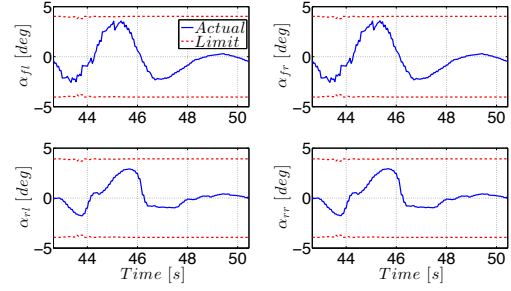
VII. EXPERIMENTAL RESULTS

A. Experimental setup description

The experiments were performed on a Jaguar S-type vehicle ($m = 2050$ kg, $I_z = 3344$ kg-m²) at the Smithers winter testing center (Raco, MI, U.S.A.) on tracks covered with packed snow ($\mu \approx 0.3$). The vehicle is equipped with an Active Front Steering (AFS) system and four wheel independent braking. An Oxford Technical Solutions (OTS)



(a) Vehicle path



(b) Slip angles at the four wheels

Fig. 4: Experimental test 1: The vehicle avoids a single obstacle with an entry speed of 80 km/hr.

RT3002 sensing system is used to measure the position and orientation in the inertial frame, and the vehicle velocities in the body frame. The OTS RT3002 system comprises of a differential GPS, an IMU and a DSP. The real-time computations are performed on a dSPACE DS1005 Autobox system which consists of a PowerPC 750GX processor running at 933 MHz. The aforementioned hardware components communicate through a CAN bus. The control actions are executed at 10 Hz.

B. Results and discussion

The following parameters are used for the controller:

- $H_p = 21$, $H_i = 3$, $N_{max} = 8$
- $e_{y,max}^{lane} = -e_{y,min}^{lane} = 5$ m
- $\delta_{f,max} = -\delta_{f,min} = 10$ deg
- $\delta_{f,max} = -\delta_{f,min} = 60$ deg/s
- $\beta_{min} = -0.5$, $\beta_{max} = 0$

Note that the value of β_{max} is 0 as the engine throttle cannot be commanded in the test vehicle. The experimental results are presented in Figures 4–6. The green lines depict the open-loop planned paths while the black line denotes the actual path of the vehicle. In the scenarios considered, the road is straight and the edge of each obstacle is at a distance of 1.5 m from the road centerline. A triangular zone is appended to the front and back of each obstacle to avoid aggressive avoidance maneuvers.

Figure 4a plots the path of the vehicle while avoiding a single obstacle at an entry speed of 80 km/hr. The vehicle stays close to the obstacle, and returns to the road centerline with a low overshoot. The slip angles at the four wheels are shown in Figure 4b. The controller is able to keep the slip

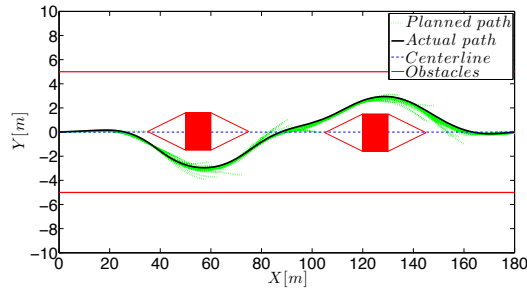


Fig. 5: Experimental test 2: The vehicle avoids two separated obstacles with an entry speed of 60 km/hr.

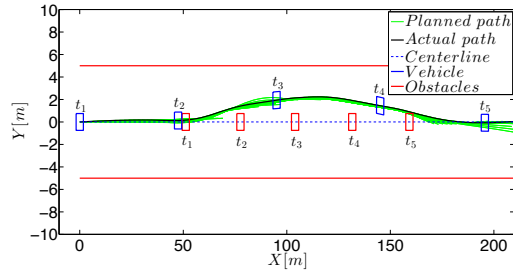


Fig. 6: Experimental test 3: The vehicle avoids an obstacle moving at 36 km/hr with an entry speed of 80 km/hr. The positions of the vehicle and the obstacle at five time instants t_1, \dots, t_5 during the test are shown.

angles within the limits. It is seen that at around $t = 45$ s, the slip angles at the front wheels are close to the limiting values (≈ 4 deg).

Figure 5 shows the path of the vehicle while avoiding two obstacles separated by a distance of 70 m. The vehicle passes the two obstacles on opposite sides due to the high-level decision making heuristic. An important point to be noted is that the number of constraints and the complexity of the optimization problems (13) and (20) are independent of the number of obstacles. This is due to the representation of obstacles by the constraint (11).

Figure 6 plots the path of the vehicle while avoiding an obstacle moving at a constant speed of 36 km/hr. The positions of the vehicle and obstacle at time instants t_1, \dots, t_5 during the test are shown. The edge of the obstacle is 1 m away from the road centerline. The lateral position of the obstacle remains constant, and it is assumed that the controller knows the present and future positions of the obstacle.

VIII. CONCLUSIONS

We have presented the design of a model-based predictive controller for an autonomous ground vehicle. A tailored algorithm based on an iterative linearization of the vehicle dynamics and convexification of the constraints is developed. It reduces the computational complexity of the online optimization problem. Experimental results at high speeds on snow demonstrate the ability of the controller to keep the vehicle safe in scenarios involving multiple obstacles and

moving obstacles. The proposed approach allows the use of much longer prediction horizons as compared to those that can be used with general purpose nonlinear solvers.

IX. ACKNOWLEDGMENTS

This material is based upon work supported by the National Science Foundation under Grant No. 1239323. Any opinions, findings, and conclusions or recommendations expressed in this material are those of the authors and do not necessarily reflect the views of the National Science Foundation. The authors acknowledge the technical support offered by Dr. Vladimir Ivanovic, Dr. Mitch McConnell and other employees of the Ford Motor Co. during the winter tests held in Racine, MI, U.S.A.

REFERENCES

- [1] R. Rajamani, *Vehicle Dynamics and Control*. Springer US, 2006.
- [2] A. Gray, M. Ali, Y. Gao, J. K. Hedrick, and F. Borrelli, "Integrated threat assessment and control design for roadway departure avoidance," in *Intelligent Transportation Systems (ITS), 2012 15th International IEEE Conference on*. IEEE, 2012, pp. 1714–1719.
- [3] A. Gray, M. Ali, Y. Gao, J. Hedrick, and F. Borrelli, "Semi-autonomous vehicle control for road departure and obstacle avoidance," in *Control in Transportation Systems, 2012 13th IFAC Symposium on*, 2012.
- [4] P. Falcone, F. Borrelli, J. Asgari, H. E. Tseng, and D. Hrovat, "Predictive active steering control for autonomous vehicle systems," *Control Systems Technology, IEEE Transactions on*, vol. 15, no. 3, pp. 566–580, 2007.
- [5] P. Falcone, F. Borrelli, H. E. Tseng, J. Asgari, and D. Hrovat, "Linear time varying model predictive control and its application to active steering systems: Stability analysis and experimental validation," *International Journal of Robust and Nonlinear Control*, vol. 18, no. 8, pp. 862–875, 2008.
- [6] J. Markoff, "Google cars drive themselves, in traffic," *The New York Times*, vol. 10, p. A1, 2010.
- [7] Y. Gao, T. Lin, F. Borrelli, E. Tseng, and D. Hrovat, "Predictive control of autonomous ground vehicles with obstacle avoidance on slippery roads," in *Dynamic Systems and Controls (DSC), 2010 3rd Annual ASME Conference on*, 2010.
- [8] Y. Gao, A. Gray, J. Frasca, T. Lin, E. Tseng, J. Hedrick, and F. Borrelli, "Spatial predictive control for agile semi-autonomous ground vehicles," in *Advanced Vehicle Control, 2012 11th International Symposium on*, 2012.
- [9] S. Anderson, S. Peters, T. Pilutti, and K. Iagnemma, "An optimal-control-based framework for trajectory planning, threat assessment, and semi-autonomous control of passenger vehicles in hazard avoidance scenarios," *International Journal of Vehicle Autonomous Systems*, vol. 8, no. 2, pp. 190–216, 2010.
- [10] P. E. Gill, W. Murray, M. A. Saunders, and M. H. Wright, "User's guide for NPSOL (Version 2. 1): a Fortran package for nonlinear programming," Stanford Univ., CA (USA). Systems Optimization Lab., Tech. Rep., 1984.
- [11] S. Han, "A globally convergent method for nonlinear programming," *Journal of Optimization Theory and Applications*, vol. 22, no. 3, pp. 297–309, 1977.
- [12] P. T. Boggs and J. W. Tolle, "Sequential quadratic programming," *Acta Numerica*, vol. 4, no. 1, pp. 1–51, 1995.
- [13] J. Nocedal and S. J. Wright, *Numerical Optimization*. Springer Verlag, 1999.
- [14] R. Hindiyeh and J. Gerdes, "Equilibrium analysis of drifting vehicles for control design," in *Dynamic Systems and Controls (DSC), 2009 2nd Annual ASME Conference on*, 2009.